GLOBAL ENGINEERS & TECHNOLOGISTS REVIEW
www.getview.org

DETERMINING FOOT-ANKLE MECHANISM DESIGN BY MAPPING THE RELATIONSHIPS AMONG BONES, JOINTS AND GROUND REACTION FORCE

A.Y., BANI HASHIM[1], N.A., ABU OSMAN[2], and W.A.B., WAN ABAS[3]

[1] Department of Robotics & Automation
Faculty of Manufacturing Engineering
Universiti Teknikal Malaysia Melaka
Hang Tuah Jaya, 76100 Durian Tunggal, Melaka, MALAYSIA
[1]yusairi@utem.edu.my

[2, 3] Department of Biomedical Engineering
Faculty of Engineering
University of Malaya
50603, Kuala Lumpur, MALAYSIA

ABSTRACT

This work investigates the following questions – why the bones and the joints are arranged in that way, why it is different from other primates, and how could it be imitated to develop a foot-ankle mechanism. Mathematical models were developed and were based on the relationship among the anatomy of bones and joints, the normalized ground reaction forces that acted on certain nodes on the footprint. Using the model, a custom design prosthetic foot was assembled. It was tested on a robot arm that simulated a walking gait. The stance phase cycle performed on the prototype, and the commercial feet were completed within approximately 1.08 seconds and 1.38 seconds respectively. The techniques used, however, may require further studies because the prototype foot was not tested on patients. At this stage, the techniques are sufficient to justify that the prototype foot design should consist of an ankle-foot mechanism and a flexible keel. Therefore, proper mappings of bones and joints; and modeling of foot biomechanics is found useful in design and development of prosthetic feet activities.

Keywords: *Ground Reaction Force, Foot Anatomy, Gait Simulator, Foot-Ankle Mechanism.*

1.0 INTRODUCTION

This work investigates the following questions—why the bones and the joints are arranged in that way, why it is different from other primates, and how could it be imitated to develop a foot-ankle mechanism (FAM). The complete set of a FAM to replace amputated foot is the prosthetic foot (PF). There were studies on foot biomechanics such as in (Wang and Crompton, 2004), and on walking gait analysis in (Elftman, 1969), (Gronley and Perry, 1984), (Krebs *et al*., 1985), (Laughman *et al*., 1984), (McGinley *et al*., 2003), (Peterson *et al*., 1985), (Su *et al*., 2007), and (Winter, 1984). Computational intelligence is the current trend in gait analysis (Lai et al., 2009). However, these studies have indirectly answered the questions posed.

On the other hand, there are ways to select commercial PF. For example, clinical teams select it by ranking of the biomechanical parameter that is the spring efficiency (Prince *et al*., 1998). Sometimes the prescribed PF is based on intuition (Twiste and Rithalia, 2003). It is argued that the current analytical technique for calculating spring efficiency has two flaws: prosthetic feet with a bendable flexible keel are analyzed the same way as those with an articulated ankle and a rigid foot; there is no accounting for the energy losses in the viscoelastic cosmetic material surrounding the keel which can be found in a silicon rubber cosmesis (Prince *et al*., 1998).

The objectives of this study are to determine the FAM design based on foot anatomy and its biomechanics through modeling of foot structure in the form of a numerical profile. The main outcome measure is to validate the three walking gait events: heel strike, mid stance, and toe-off of the prototype FAM. The performance test was performed using COMAU robot that simulated human gait. The outcome measures of the prototype FAM and a PF will be compared.

2.0 METHOD

2.1 Expanding from the Foot Anatomy

Bones and joints of human foot have a complex arrangement. The interconnectedness of the bones and joints forms an effective actuator (foot), where walking gait for human is completely different to other primates. Using this arrangement as a reference, we developed a graph that charted bones and joints localities after a kinematic structure was created. Kinematic structure is an abstract representation of a mechanical structure. It contains the essential information about which link (L) connects to which other links by what types of joint (J). Figure 1 shows the proposed kinematic structure that represents the human foot. We have, L_1 connects L_2 and L_3 where L_1 represents talus bone. An object shape represents a type of link. The legends on the right-hand side of Figure 1 name the meaning of the object shapes found in the figure. For example, L_1 is a quaternary link. There are three different types of links: quaternary, ternary, and binary. A quaternary link has four joints. The ternary has three, and the binary has two. A circle represents a revolute single-axis joint. The two shaded circles are the joints that connect the talus to fibula and tibula. These bones provided insignificant applications this study.

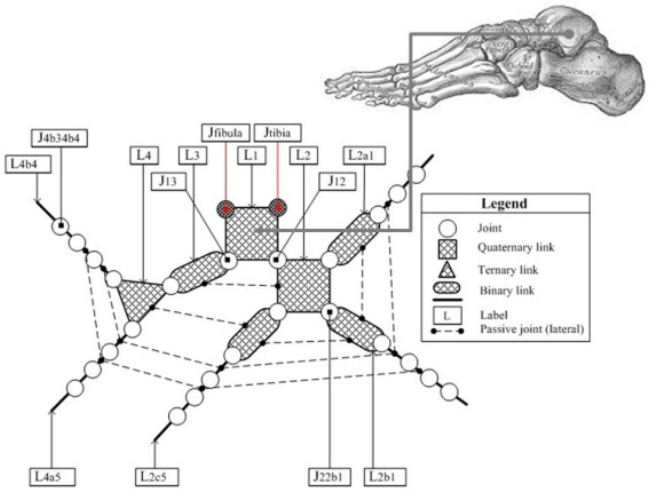

Figure 1: The proposed human foot kinematic structure is shown above. The legends explain the object symbols that represent the bones and joints, for example, L_1 represents the talus.

A network of vertices forms a graph. Graphs can aid the process of mechanical structures design (Tsai, 2001). In general, a graph contains vertices and edges. In Figure 2, the circles represent the vertices (V), the connecting lines represents the edges E , and the concentric circle is the root—talus (v_1). In fact, these are the conversions of the links and the joints of Figure 1 where a link is equivalent to a vertex and a joint to an edge. The labels designate the locations of the vertices and the edges. For example, v_{2a1} follows v_2 and e_{22a1} connects v_2 to v_{2a1} . The degree of vertex is equivalent to the number of edges. Equation (A.1) defines the vertex-to-vertex adjacency. It is an $N_V \times N_V$ symmetric matrix having zero diagonal elements. Equation (A.2), however, defines a matrix that outlines the incidences of the vertices and the edges. Lastly, equation (A.3) defines the path matrix that stores information about all paths that emanate from the root. It is an $N_{\mathrm{E}} \times \left(N_{\mathrm{V}} - 1\right)$ matrix excluding the root.

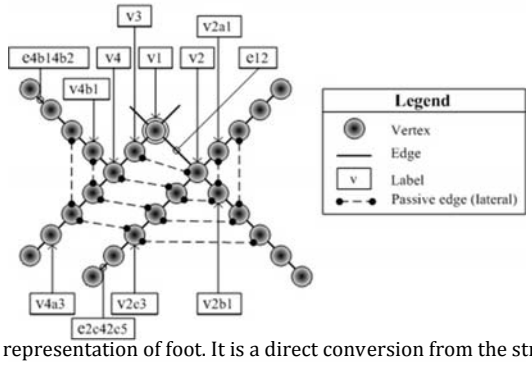

Figure 2: Above is the graph representation of foot. It is a direct conversion from the structural kinematics. The legend names each of the object symbols.

Due to large sizes, where **A** is 26×26, **B** is 26×25, and **P** is 25×25, the matrices are not included in this paper. If one is to inspect the matrix, the element $a_{12}=1$ indicates that v_2 is adjacent to v_1. The elements a_{23}, a_{24}, and a_{25} are adjacent to the common vertex that v_{2a1}, v_{2b1}, and v_{2c1} are adjacent to v_2. It signifies a quaternary link. Similarly, $a_{19,8}=1$ and $a_{19,9}=1$ show that v_{4a1} and v_{4b1} are adjacent to v_4. It is a ternary link. There is zero diagonal that implies none of the vertices mirrored itself. Every column has a pair of elements that indicates incidences of the vertices and the edges. In row two of **B** there are four incidences and in row nineteen there are three. The remaining rows have two incidences. Four incidences signify the occurring vertex has four edges. The size of **P** is 25×25. The patterns of the elements arrangement in **P** describe the sequences of trail, path, and walk found in the graph.

Equations (A.1) to (A.3) contain information concerning the foot architecture. We altered the equations into equations (A.4) to (A.6) so that these can be visualized as in Figure 3. These are the characteristic images formatted in grayscale. The grayscale has the scale of natural numbers 0 until 255. The digit 0 characterizes pure black, whereas 255 pure white. The α, β, and π are the variables for manual assignments of the scale. The images produced using these equations would have apparent pixels as depicted in Figure 3.

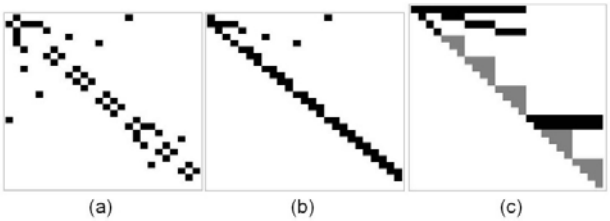

Figure 3: The characteristic images: **(a)** Vertex-to-Vertex adjacency, **(b)** Vertex-to-Edge incidence, and **(c)** Paths that emanates from the root.

Figure 3 (a), $\mathbf{A}_{\text{IMAGE}}$ has 676 pixels. The element $a_{\text{IMAGE},1,2}=0$ where a pure black pixel indicates v_2 is adjacent to v_1. In other words, talus borders calcaneus. The pure white diagonal implies that none of the vertices mirrored itself. The $\mathbf{A}_{\text{IMAGE}}$ has an "←" shape. Similarly, Figure 4 (b), $\mathbf{B}_{\text{IMAGE}}$ has 650 pixels. In the row-column intersections, the vertices and the edges meet. In row two, there are four black pixels that indicate four incidences. In row nineteen, there are three, and in the remainders there are two. The $\mathbf{B}_{\text{IMAGE}}$ has a "ے" shape. Figure 3c, $\mathbf{P}_{\text{IMAGE}}$ has 625 pixels. The five light gray triangles that represent the foot's five digits. Five-digit foot is a common primate's feature. The image describes the possible paths, walks, and trails that emanate from the root and terminate at v_{j+1}. A trail, however, can have only unique elements. This distinguishes a path from a trail. For example, in Trail-1 the sequence begins from e_{22a1} terminates at v_{2a4} —the first triangle in Figure. 3 (c), whereas Path-1 begins from v_2 and terminates at v_{2a4}.

2.2 Expanding from Foot Bimechanics

By inspection, human foot has twenty-seven bones. It has five digits known as the phalanges. The phalanges control of the drop-off phenomenon—the experience at the end of the stance phase. Calcaneus, on the other hand, works upon the initial contact with the ground. It is the largest bone that bears body weight on heel strike. Navicular and cuboid bear distributed body weight on foot flat.

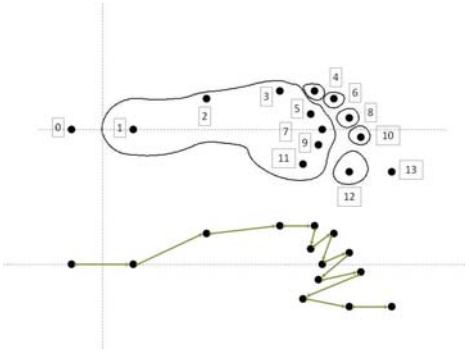

Figure 4: Above—there are twelve nodes on a footprint, and two nodes that represent the points prior to heel strike and the point just after toe-off during stance. Below—the connecting lines form a gait path that a stance phase should follow.

The end phalanx or the toe bears the body weight at the concluding of the stance phase. Let there be a number of sequences from the point-of-contact (POC) POC-0 to POC-13 during walking gait. The sequence Q is dependent on the moments when the POCs meet the ground. Every sequence has at least one POC and some degree of the ground reaction force (GRF— f_k) except for Q_0 and Q_{13} . On foot flat, there are twelve POCs and it is depicted in Figure 4.

$$\mathbf{H} = \begin{bmatrix} A & A & A & A & A & A & A & A & A & A & A & A & A & A \\ A & V & A & A & A & A & A & A & A & A & A & A & A & A \\ A & V & L & L & M & M & M & S & S & S & S & S & S & A \\ A & A & V & L & L & M & M & M & S & S & S & S & S & A \\ A & A & A & V & L & L & M & M & M & S & S & S & S & A \\ A & A & A & A & V & L & L & M & M & M & S & S & S & A \\ A & A & A & A & A & V & L & L & M & M & M & S & S & A \\ A & A & A & A & A & A & V & L & L & M & M & M & S & A \\ A & A & A & A & A & A & A & V & L & L & M & M & M & A \\ A & A & A & A & A & A & A & A & V & L & L & M & M & A \\ A & A & A & A & A & A & A & A & A & V & L & L & M & A \\ A & A & A & A & A & A & A & A & A & A & V & L & L & A \\ A & A & A & A & A & A & A & A & A & A & A & V & L & A \\ A & A & A & A & A & A & A & A & A & A & A & A & V & A \\ A & A & A & A & A & A & A & A & A & A & A & A & A & A \end{bmatrix} \quad (1)$$

It is straightforward that POC-0 during Q_0 does not experience any reaction prior to touching the ground. In this sequence, none of the POCs has contact with the ground. This is also true for the last sequence. However, upon initial contact with the ground, POC-1 bears maximum body load where with $f_k \rightarrow V$. Equation (1) defines the degrees of GRF upon contact with the ground during specific sequences that follow the gait path. The rows stand for the sequences and the columns stand for the POCs. The degree 'V' means "very large", 'L' is "large", 'M' is "medium", 'S' is "small", and 'A' is "absent". During Q_0 , there is no GRF and Q_1 has "very large" GRF. We proposed that for an ideal stance, the estimated degree of GRF of the walk in graph versus the walk in graph has an M-shaped curve shown in Figure 5. We suggested that the peaks on the curve signified the sequences on heel strike and on toe-off respectively, whereas the valley signified the sequence on mid stance.

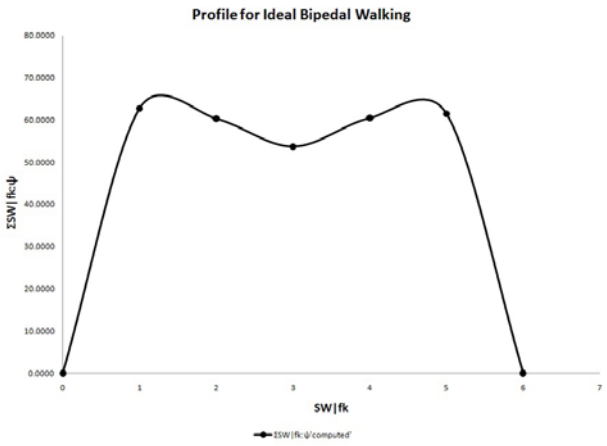

Figure 5: The profile for ideal stance phase derived from Eq. (1) and reproduction from (Bani Hashim *et al.,* 2011).

3.0 RESULTS

A healthy and normal 25-year-old male subject, weighed approximately 70–kilograms participated in this study. The subject's right foot was scanned using a computer scanner. The twelve POCs were marked on the locations suspected to be the areas of high concentration of GRFs on a stand posture. The distance among the nodes were measured and recorded. The locations of the points were compared with the gait path where the curve and the image were superimposed to show this relationship (Figure 6). The first curve's peak seemed to concentrate around POC-2, while the second peak seemed to concentrate around POC-11. In Figure 7 are three functions positioned on the top, the middle, and the lowest; $\Gamma_0(\mathrm{POC},\mathrm{D_A})$, $\Gamma_1(\mathrm{POC},0.5\mathrm{D_A})$, $\Gamma_2(\mathrm{POC},0.25\mathrm{D_A})$ respectively. The curves of Figure 7 were derived from the measured distances of the POCs from the origin. The function Γ_1 was estimated halve of the initial function, Γ_0. Similarly, the function Γ_2 was taken quarter of the initial function that yielded to the estimated points: POC-3e, POC-7e, and POC-11e. As a result, these points provided the length parameters required to fabricate the FAM as shown in Figure 8.

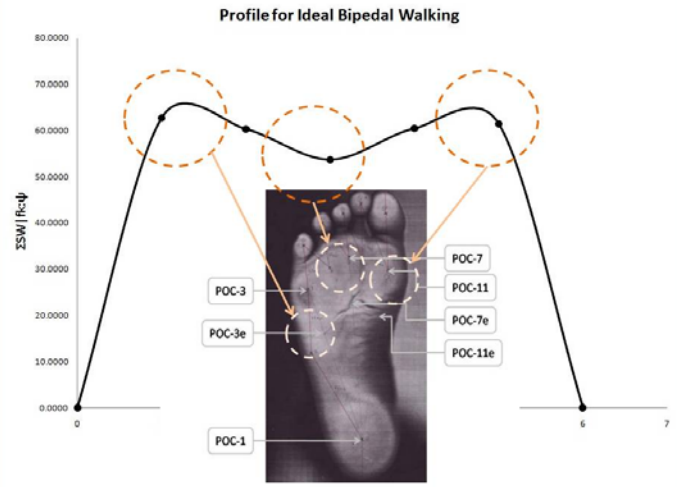

Figure 6: The scanned image of the subject's right foot. The points were marked on the image. The effective points were found to be related to the peaks and the valley of the gait path.

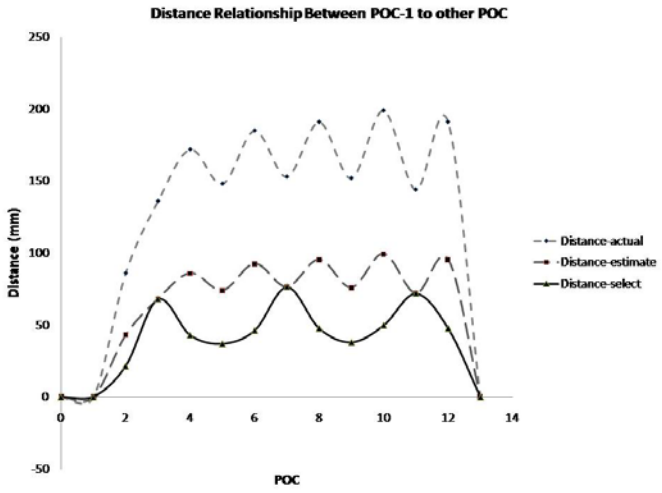

Figure 7: The estimated functions for the effective POCs.

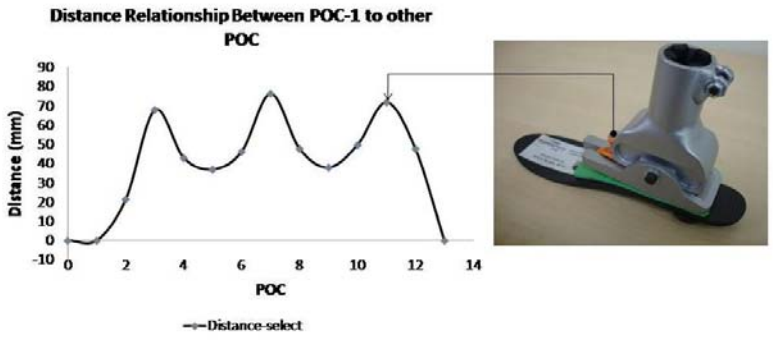

Figure 8: The relationship between the estimated curve and the actual construction of the FAM.

In addition, the FAM's overall construction needed some design justifications. The justifications were made based on the characteristic images shown in Figure 9. The adjacency image of Figure 9 (a), the gray pixels (α=128) represented the occurring f_k on stance phase. This depiction detailed the effective vertices, hence the bones. Further, Figure 9 (b) shows the occurring vertices where GRFs were subjected on points nearby certain edges depicted by the vertex-to-edge incidences in gray pixels (β=128). Figure 7 (c), however, the image considered the useful sequences of the f_k on stance phase derived from Fig. 9 (a) and Fig. 9(b). Therefore, the top left object in Figure 9 (c) was the foot-ankle module. The loose objects were the remaining components that made the prototype PF (Figure 10). One of the components was a flexible keel.

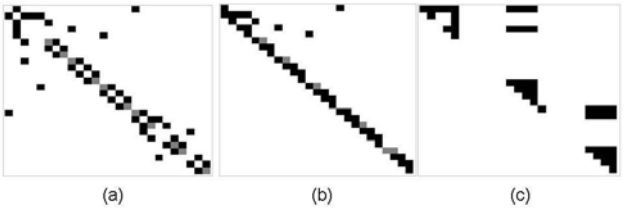

Figure 9: The characteristic images: **(a)** The adjacency image showing the vertices in gray pixels (α=128) where f_k existed; **(b)** the incidence image showing vertex-to-edge incidences in gray pixels (β=128) where f_k existed; **(c)** the path image showing vertex-to-edge paths where the FAM components were identified.

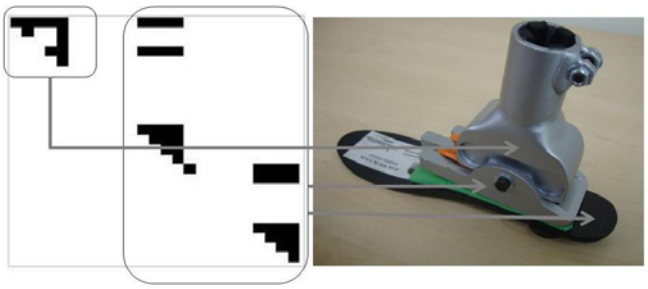

Figure 10: The laboratory prototype PF design that was constructed based on the proposed numerical profile.

The experiment setup is shown in Figure 11 where the COMAU manipulator was used to simulate an artificial walking gait. The robot was trained several times and the best program was chosen to be executed for the artificial walking gait. An industrial robot was used to simulate gait because it could provide consistent motion with loads. In addition, it replaced human subject to test a prototype PF. A force plate system was used to read and to record the normalized vertical GRF as the feet were subjected to loads during simulations. Some 70-kg was applied by the robot to suit the subject's weight. The sequence shots of the simulated walking gait with the prototype and the commercial feet are shown in Figure 12. The stance phase cycle (Figure 13) performed on the prototype PF and the commercial foot were completed within approximately 1.08 seconds and 1.38 seconds respectively. For the prototype PF, the curve's pattern depicted the three events: the heel strike at 0.74 seconds from initial contact, the mid stance at 0.20 seconds after heel strike, and the toe-off at 0.14 seconds after mid stance. Similarly, for the commercial PF, the curve's pattern depicted the heel strike at 1.08 seconds from initial contact, the mid stance at 0.14 seconds after heel strike, and the toe-off at 0.16 seconds after mid stance.

Figure 11: Above is an adaptation of an industrial robot to simulate an amputee's stance phase. Although the accuracy of this approach may be questionable it did provide a means through which the prototype FAM could be tested without the need for the involvement of an amputee.

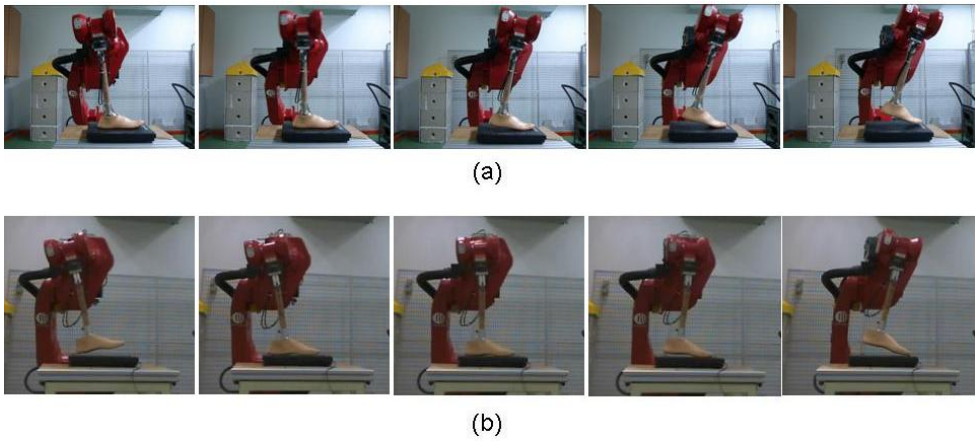

Figure 12: The simulated stance was tested on **(a)** commercial PF, **(b)** laboratory prototype PF.

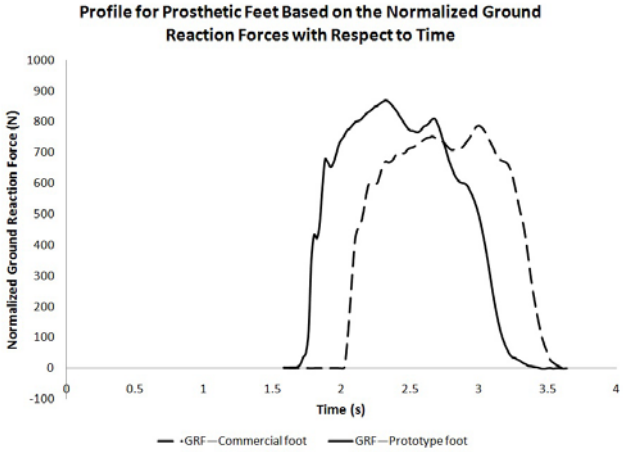

Figure 13: Above are the profiles of the normalized GRF for the prototype foot and the commercial foot.

4.0 DISCUSSION AND CONCLUSION

There is no common method for PF design method. It is important that PF is designed and developed with the considerations that it resembles to a normal human foot in terms of outlooks as well as functionality. The outcomes of this work proved that proper study of foot structure may result in a justifiable PF outlook, and modeling of foot biomechanics may result in an acceptable PF functionality. The techniques used, however, may require further studies because the prototype PF was not tested on patients. At this stage, the techniques are sufficient to justify that the PF design should consist of an ankle-foot mechanism and a flexible keel. In addition, the method to construct PF based on the scanned foot image was proposed. It was derived from the unique structural foot modeling. This approach promises a fast and low-cost option for design of PF. It is possible because the process simply requires the patient who has undergone transtibial amputation to submit the scanned foot image of scale 1:1 to the clinician. The clinician will communicate with engineers whom will then use the relevant information to estimate a custom-design PF according to the proposed methods. The clinicians may prescribe PF following this process, in addition to, their intuition and experience. In fact, it is straightforward for engineers to decide on the construction and manufacturing matters. Moreover, local materials may be considered in fabricating the device to achieve a low-cost production. For example, fibers derived from coconut trees are abundant in South-East Asia that could be used to as supplemental materials for PF fabrication. In fact, Yuhazri et al. (2011) have proven that coconut fibers may be applied as heat insulators. The patients, on the other hand, may order a custom-design PF online and perform a self-installation, if necessary. Therefore, a proper mapping of bones and joints; and modeling of foot biomechanics is found useful in design and development of prosthetic feet activities.

ACKNOWLEDGMENTS

This work was supported in part by the Malaysian Ministry of Higher Education under Grant FRGS/2008/FKP-0069.

REFERENCES

[1] Bani Hashim, A.Y., Abu Osman, N.A. and Wan Abas, W.A.B. (2011): Prosthetic Foot Design: The Significance of the Normalized Ground Reaction Force. In Abu Osman, N.A., Wan Abas, W.A.B., Abdul Wahab A.K., and Ting, H.-N. (Eds.), *5th Kuala Lumpur International Conference on Biomedical Engineering* (Vol. 35, pp. 765-768). Kuala Lumpur, Malaysia: IFMBE Proceedings.

[2] Elftman, H. (1969): Dynamic Structure of the Human Foot. *Artificial Limbs, 13*, pp. 49-58.

[3] Gronley, J.K. and Perry, J. (1984): Gait Analysis Techniques. *Physical Therapy, 64*, pp. 1837-1838.

[4] Krebs, D.E., Edelstein, J.E. and Fishman, S. (1985): Reliability of Observational Kinematic Gait Analysis. *Physical Therapy, 65*, pp. 1027-1033.

[5] Lai, D.T.H., Begg, R.K., and Palaniswami, M. (2009): Computational Intelligence in Gait Research: A Perspective on Current Applications and Future Challenges. *IEEE Transactions on Information in Biomedicine, 13*, pp. 687-702.

[6] Laughman, R.K., Askew, L.J., Bleimeyer, R.R and Chao, E.Y. (1984): Objective Clinical Evaluation of Function Gait Analysis. *Physical Therapy,* pp. *64*.

[7] McGinley, J.L., Goldie, P.A., Greenwood, K.M. and Olney, S.J. (2003): Accuracy and Reliability of Observational Gait Analysis Data: Judgments of Push-off in Gait After Stroke. *Physical Therapy, 83*, pp. 146-160.

[8] Peterson, M.J., Perry, J. and Montgomery, J. (1985): Walking Patterns of Healthy Subjects Wearing Rocker Shoes. *Physical Therapy, 65*, pp. 1483-1489.

[9] Prince, F., Winter, D.A., Sjonnensen, G., Powell, C. and Wheeldon, R.K. (1998): Mechanical Efficiency During Gait of Adults with Transtibial Amputation: A Pilot Study Comparing the SACH, Seattle, and Golden-Ankle prosthetic feet. *Journal of Rehabilitation Research and Development, 35*, pp. 177-185.

[10] Su, P.-F., Gard, S.A., Lipschutz, R.D. and Kuiken, T.A. (2007): Gait Chracteristics of Person with Bilateral Transtibial Amputations. *Journal of Rehabilitation Research and Development, 44*, pp. 491-502.

[11] Tsai, L.W. (2001): *Mechanism Design: Enumeration of Kinematic Structure Accoring to Function*. Boca Raton, Florida: CRC Press.

[12] Twiste, M. and Rithalia, S. (2003): Transverse Rotation and Longitudinal Translation During Prosthetic Gait-A literature Review. *Journal of Rehabilitation Research and Development, 40*, pp. 9-18.

[13] Wang, W.J. and Crompton, R.H. (2004): Analysis of the Human and Ape Foot During Bipedal Standing with Implications for the Evolution of the Foot. *Journal of Biomechanics, 37*, pp. 1831-1836.

[14] Winter, D.A. (1984): Kinematics and Kinematics Patterns in Human Gait. *Human Movement Science, 3*, pp. 51-76.

[15] Yuhazri, M.Y., Sihombing, H., Jeefferie, A.R., Ahmad Mujahid, A.Z., Balamurugan, A.G., Norazman, M.N., Shohaimi, A. (2011): Optimazation of Coconut Fibers Toward Heat Insulator Applications. Global Engineers & Technologists Review, Vol. 1 No. 1, pp. 35-40.

APPENDIX

$$\mathbf{A}=\left\{\left[a_{i,j},N_{\mathrm{V}}\times N_{\mathrm{V}}\right]\;\middle|\;\left(a_{i,j}=\begin{cases}1 & \text{if } v_i \text{ is adjacent to } v_j\\ 0 & \text{otherwise and } i=j\end{cases}\right);v\in V\right\} \tag{A.1}$$

$$\mathbf{B}=\left\{\left[b_{i,j},N_{\mathrm{V}}\times N_{\mathrm{E}}\right]\;\middle|\;\left(b_{i,j}=\begin{cases}1 & \text{if } v_i \text{ contain } e_j\\ 0 & \text{otherwise}\end{cases}\right);v,e\in V,E\right\} \tag{A.2}$$

$$\mathbf{P}=\left\{\left[p_{i,j},N_{\mathrm{E}}\times\left(N_{\mathrm{V}}-1\right)\right]\;\middle|\;\left(p_{i,j}=\begin{cases}1 & \text{if } e_{i,j} \text{ lies on the path, end at } v_{j+1}\\ 0 & \text{else}\end{cases}\right);e,v\in E,V\right\} \tag{A.3}$$

$$\mathbf{A}_{\mathrm{IMAGE}}=\left\{\left[a_{\mathrm{IMAGE},i,j}\right]\;\middle|\;\left(a_{\mathrm{IMAGE},i,j}=\begin{cases}0 & \text{if } a_{i,j}=1\\ \alpha & \text{open}\\ 255 & \text{if } a_{i,j}=0\end{cases}\right);a_{\mathrm{IMAGE},i,j}\in\square\right\} \tag{A4}$$

$$\mathbf{B}_{\mathrm{IMAGE}}=\left\{\left[b_{\mathrm{IMAGE},i,j}\right]\;\middle|\;\left(b_{\mathrm{IMAGE},i,j}=\begin{cases}0 & \text{if } b_{i,j}=1\\ \beta & \text{open}\\ 255 & \text{if } b_{i,j}=0\end{cases}\right);b_{\mathrm{IMAGE},i,j}\in\square\right\} \tag{A.5}$$

$$\mathbf{P}_{\mathrm{IMAGE}}=\left\{\left[p_{\mathrm{IMAGE},i,j}\right]\;\middle|\;\left(p_{\mathrm{IMAGE},i,j}=\begin{cases}0 & \text{if } p_{i,j}=1\\ \pi & \text{open}\\ 255 & \text{if } p_{i,j}=0\\ \tau & \text{else, } \tau\neq\pi\end{cases}\right);p_{\mathrm{IMAGE},i,j}\in\square\right\} \tag{A.6}$$